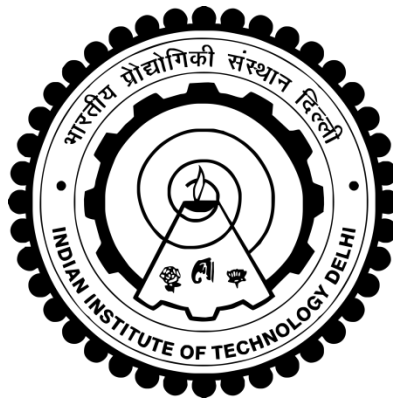


**DESIGN, DEVELOPMENT, AND CONTROL OF  
INDUCTION MOTOR DRIVE WITH INVERTER  
OUTPUT LC FILTER**

**PRASUN MISHRA**



**DEPARTMENT OF ELECTRICAL ENGINEERING  
INDIAN INSTITUTE OF TECHNOLOGY DELHI  
APRIL 2020**

©Indian Institute of Technology Delhi (IITD), New Delhi, 2020

**DESIGN, DEVELOPMENT, AND CONTROL OF  
INDUCTION MOTOR DRIVE WITH INVERTER  
OUTPUT LC FILTER**

**by**

**PRASUN MISHRA**

**Department of Electrical Engineering**

*Submitted*

*in fulfillment of the requirements of the degree of Doctor of Philosophy*

**to the**



**INDIAN INSTITUTE OF TECHNOLOGY DELHI**

**APRIL 2020**

## CERTIFICATE

It is certified that the thesis entitled “**Design, Development, and Control of Induction Motor Drive with Inverter Output LC Filter,**” being submitted by **Mr. Prasun Mishra** for award of the degree of **Doctor of Philosophy** in the Department of Electrical Engineering, Indian Institute of Technology Delhi, is a record of the student work carried out by him under my supervision and guidance. The matter embodied in this thesis has not been submitted for the award of any other degree or diploma.

**Dated: 17. 04. 2020**



**( Dr. Ramkrishan Maheshwari )**

**Associate Professor  
Department of Electrical Engineering  
Indian Institute of Technology Delhi  
Hauz Khas, New Delhi-110016, India**

## **ACKNOWLEDGEMENTS**

I wish to express my sincere and heartfelt gratitude to my supervisor, Dr. Ramkrishan Maheshwari, for the fruitful technical discussions, indispensable suggestions, and motivations which really invigorated me to overcome the hurdles in my doctoral research work. He always asked me to do a thorough analysis of the research problems to find meaningful solutions supported by mathematical and experimental validations, and steered me in the right co-ordinate. It was really a great opportunity to work under his skillful guidance on the trending research areas which finally opened the doors of the illuminated research world for me and made me believe in myself.

I am grateful to my SRC members, Prof. M. Veerachary, Dr. Amit Kumar Jain, and Dr. Ashu Verma, for evaluating my research work critically in every semester and giving valuable suggestions which really helped me to grow through with time. I want to thank Dr. Deepak Patil for a few fruitful technical sessions and suggestions. I also convey my regards to Prof. Bhim Singh, Prof. G. Bhuvaneshwari, and Dr. Anandarup Das for their encouragement and support.

I am thankful to the staff of the PG Section, Account Section, Purchase and Store Section, Industrial R&D Unit, Central Library, and Departmental Office. I extend my immense gratitude to MHRD for monthly fellowship and SERB for funding the research expenditures. I extend my thanks to the staff (Mr. Dhanraj Singh and others) of UG Drives Lab and registered vendors for providing me the facilities and assistance timely. I would like to thank the staff of Jwalamukhi Hostel, Security Section, Scoops, Xerox Center, refreshment shops, and others for their convenient affairs and support.

The healthy work culture of UG Drives Lab of IIT Delhi has been a great pleasure to me. I would like to thank my associates (Mr. Navneet Vaishnav, Mr. Nikhil Krishna, Mr. Aamir Rafiq, Mr. Rahul Sharma, Mr. Himanshu Swami, Mr. Martin Cheerangal, Miss Nibedita Parida, Miss Nidhi Bist, Miss Khushboo Kumari, Miss Chesta Jain, Miss Apurva Verma, and others) and the alumni of UG Drives Lab (Dr. Kapil Shukla, Dr. Himanushu Mishra, Mr. Navneet Mangal, Mr. Gaurav Kumar, Mr. Thakur Sumeet Singh, Mr. Phani Sekhar Chennu, Mr. Sourabh Khandelwal, Mr. Rakesh Panda, Mr. Amit Kumar Kandi, Mr. Sritam Jena, and others) for their encouragement and support during my doctoral study. I also thank Dr. Sayan Basu Roy and Mr. Joyjit Mukherjee for a few doubt clarification sessions on control theory. I really want to mention the name of my

friends (Dr. Nishant Kumar, Mr. Anshul Varshney, Mr. Anjanee Mishra, Mr. Piyush Kant, Mr. Priyank Shah, Mr. Sreejith Raveendran, Mr. Tripurari Nath Gupta, Mr. Nikhil Kumar, Mr. Shrikant Misal, Mr. Saurabh Shukla, Mr. Akash Jain, and others), and juniors (Mr. Siddhartha Sarkar, Mr. Dhiman Das, Mr. Priyabrata Shaw, Mr. Punit Kumar Singhal, Mr. Ambuj Sharma, Mr. Shubham Sundeep, Mr. Bipin Patel, Mr. Purnashis Chakraborty, and the members of Basanta Utsab Samity of IIT Delhi) for making my stay enjoyable, hassle-free and memorable at IIT Delhi.

Finally, I wish to express my heartfelt profound respect, indebtedness, and intense love to my parents, siblings, teachers and my well-wishers for their blessings, love, affection, sacrifice, and co-operation to bring me up to this level.



Date: 17. 04. 2020

Prasun Mishra

## ABSTRACT

Pulse-width modulated (PWM) three-phase (3-ph) voltage source inverter (VSI) fed 3-ph squirrel cage induction motor (SQIM) drive has been evolved into a matured and widely accepted technology through uninterrupted research works carried out over time. It has been widely used in various domestic and industrial constant or adjustable speed drives where the motor drive has to meet a constant or dynamic speed and torque demands of the load in a controlled manner based on the application requirements. In recent time, the superior material properties of silicon-carbide (SiC) over silicon (Si) have emerged the possibilities of using SiC power semiconductor devices in place of the prolonged Si power semiconductor devices used in the VSI. The SiC power device has the capabilities of blocking higher voltage, withstanding higher temperature, and switching at higher switching frequency with lower switching losses than the existing Si power device and thus it helps to increase the power density as well as efficiency of the VSI especially at medium and high power drives and also to reduce the cooling requirements. However, the cost of the SiC devices is still quite high as compared to the cost of Si devices and the power semiconductor device manufactures are trying to reduce it as much as possible.

However, the fast turn on and fast turn off features of the SiC devices in such high switching frequency operation make the design and printed circuit board (PCB) layout of dc-bus bar, gate driving circuits, protection circuits, sensing circuits of the SiC VSI quite challenging because of the presence of parasitic inductances and capacitances in different paths of the circuits. Therefore, a 5 kVA SiC MOSFETs based two-level 3-ph VSI have been designed, developed in-house as a part of this research work. The developed VSI has mainly three parts such as Power and Sensor Circuits (PSC), Gate Driver and Protection Circuits (GDPC), and Control Interface and Signal Conditioning Circuits (CISCC). The developed SiC VSI been successfully tested with an open-loop  $v/f$  controlled 3-ph SQIM with load at 5 kHz and 50 kHz switching frequencies and its performance has been evaluated. TMS320F28335 has been used as a digital signal controller for implementing the algorithm of open-loop  $v/f$  control. The steady-state temperature of the heat-sink of the VSI with natural and forced cooling has been measured by a thermocouple while the VSI continuously drives the SQIM for 90 minutes.

Space-vector pulse-width modulation technique is generally used in a two-level VSI fed SQIM drive mainly for better dc-bus utilization. However, the PWM output voltages of the VSI mainly

contain fundamental frequency component, higher-order harmonics in the sideband of the carrier or switching frequency, and certain low order harmonics because of the dead-time used in the VSI to prevent shoot-through. These higher-order switching harmonics mainly incur core losses (hysteresis and eddy current loss) and temperature rise inside the motor, and thus reduce the overall efficiency of the SQIM drive. The rate of rise ( $dv/dt$ ) of the stator-voltages of the SQIM increases significantly because of the fast switching transients of the device with high dc-link voltage. It basically aggravates the chances of winding insulation failure, bearing current, electromagnetic magnetic interference issues, etc. Therefore, sinusoidal LC filter network is used in between the VSI and SQIM to make the motor input voltages sinusoidal by attenuating higher-order harmonics present in the pulse-width modulated output voltages of the VSI. It also increases the life of the motor by drastically reducing the fast switching transients of the motor input voltages. In this research work, a new methodology of designing a sinusoidal LC filter is proposed for a PWM VSI fed SQIM drive where the filter capacitance is chosen based on the reactive power demand of the SQIM at its rated frequency. However, the calculation of filter inductance in the proposed filter design method (PFDM) is similar to the calculation of filter inductance in the standard filter design method (SFDM). The proposed LC filter serves the purpose of a sinusoidal filter, reduces the  $dv/dt$ , and also supplies the reactive power demand of the SQIM and thus reduces the inverter output currents. The impacts of the LC filter designed by SFDM and PFDM on the magnitude of switch current, losses in the drive, temperature of dc-link capacitor,  $dv/dt$  at motor terminal, stator flux, and air-gap torque of the SQIM are analyzed with apposite simulation and experimental results. The experiments have been performed in an experimental set-up where the developed VSI is switching at 50 kHz and driving a SQIM in open loop  $v/f$  control at different test conditions. The proposed methodology can be used to design a sinusoidal LC filter for any VSI made of Si IGBTs or SiC MOSFETs switching at 5 kHz or 50 kHz.

SQIM drive without LC filter in rotor-flux oriented control (RFOC) is a stable closed-loop system at different operating points if two inner-loop and two outer-loop controllers are designed properly. However, the introduction of LC filter in between the VSI and the SQIM may make the closed-loop system unstable at different operating points when the parameters of the previously designed controllers for RFOC of SQIM without the filter are not changed. Therefore, the instability of the closed-loop drive at different operating points has been analyzed with the same controller parameters and it has been observed that such instability occurs due to high amplitude

resonance frequency oscillations. Therefore, four different active damping (AD) methods have been proposed to stabilize those unstable operating points by damping out the resonance frequency oscillations without incurring any active power loss. However, all these AD methods do not change the basic control structure of RFOC of SQIM and the parameters of the previously designed proportional-integral (PI) controllers of RFOC of SQIM without the filter.

The performance of the first two AD methods in RFOC of SQIM with LC filter is dependent on the proper calculation of damping gain in AD Method I using inverter-currents or gain matrix in AD Method II using LQR. In these two AD methods, compensating terms have been subtracted from the output voltage references of the inner-loop current controllers to damp out the resonance frequency oscillations without incurring any active power loss. However, multiple high-pass filters have been used for extracting resonance frequency components from the sensed state variables of the drive and the compensating terms are formulated. Moreover, these AD methods require additional sensors for sensing the inverter-currents or the voltages across the filter capacitors apart from the sensors used in RFOC of SQIM without filter.

However, AD Method III and Method IV, there is no need for additional sensors, tedious calculation of damping gain or gain matrix, high-pass filters for resonance frequency extraction. The AD Method III basically subtracts two feed-forward terms from two current references of the inner stator-current loops in RFOC of SQIM with the filter to stabilize the unstable operating points. The AD Method IV basically introduces time delay and modifies the inner stator-current loops to stabilize the unstable operating points. The performances of the drive with these methods have also been verified w.r.t the parametric variation of the system. Theoretical analysis, multiple simulation results, and experimental results have been presented at different test conditions of the drive to validate the effectiveness of four AD methods confirming satisfactory steady-state and dynamic performance of the SQIM drive with the filter.

## सार

पल्स-चौड़ाई मॉड्युलेटेड (पीडब्लूएम) तीन-चरण (3-ph) वोल्टेज स्रोत इन्वर्टर (VSI) खिलाया 3-ph गिलहरी पिंजरे प्रेरण मोटर (SQIM) ड्राइव को एक परिपक्व और व्यापक रूप से स्वीकार किए गए प्रौद्योगिकी पर निर्बाध शोध कार्यों में विकसित किया गया है। यह विभिन्न घरेलू और औद्योगिक निरंतर या समायोज्यगति ड्राइव में व्यापक रूप से उपयोग किया गया है जहां मोटर ड्राइव को एप्लिकेशन आवश्यकताओं के आधार पर नियंत्रित तरीके से लोड की एक निरंतर या गतिशील गति और टोक मांगों को पूरा करना है। हाल के समय में, सिलिकॉन (कार्ब) से अधिक सिलिकॉन (कार्ब) (SiC) के श्रेष्ठ भौतिक गुणों ने VSI में प्रयुक्त लंबे समय तक Si पॉवर सेमीकंडक्टर उपकरणों के स्थान पर SiC पॉवर सेमीकंडक्टर उपकरणों का उपयोग करने की संभावनाओं को उभारा है। SiC पावर डिवाइस में उच्च वोल्टेज को अवरुद्ध करने, उच्च तापमान को समझने, और मौजूदा स्विचन के साथ कम स्विचिंग आवृत्ति पर स्विच करने की क्षमता होती है, जो मौजूदा Si पॉवर डिवाइस की तुलना में कम होती है और इस प्रकार यह पावर डेंसिटी और साथ ही VSI की दक्षता को बढ़ाने में मदद करती है। मध्यम और उच्च शक्ति ड्राइव और शीतलन आवश्यकताओं को कम करने के लिए भी। हालांकि, SiC उपकरणों की लागत अभी भी काफी अधिक है क्योंकि Si डिवाइसों की लागत और पावर सेमीकंडक्टर डिवाइस मैनुफैक्चरर इसे ज्यादा से ज्यादा कम करने की कोशिश कर रहे हैं।

हालांकि, इस तरह के उच्च स्विचिंग आवृत्ति ऑपरेशन में SiC उपकरणों की तेज़ गति और तेज़ी से बंद सुविधाएँ, डीसी-बसबार, गेट ड्राइविंग सर्किट, सुरक्षा सर्किट, SiC के संवेदन सर्किट का डिज़ाइन और मुद्रित सर्किट बोर्ड (PCB) लेआउट बनाती हैं। सर्किट के विभिन्न रास्तों में परजीवी अधिष्ठापन और समाई की उपस्थिति के कारण वीएसआई काफी चुनौती पूर्ण है। इसलिए, 5 kVA SiC MOSFETs आधारित दो-स्तरीय 3-ph VSI को डिज़ाइन किया गया है, जो इस शोध कार्य के एक भाग के रूप में विकसित किया गया है। विकसित VSI में मुख्य रूप से तीन भाग होते हैं जैसे पावर और सेंसर सर्किट (PSC), गेट ड्राइवर और प्रोटेक्शन सर्किट (GDPC), और कंट्रोल इंटरफेस और सिग्नल कंडीशनिंग सर्किट (CISCC)। सेंसर सर्किट में तीन-चरण मोटर धाराओं को संवेदन के लिए तीन वर्तमान सेंसर और डीसी-लिंक वोल्टेज को संवेदन के लिए एक वोल्टेज सेंसर होता है। विकसित SiC VSI को एक ओपन-लूप  $v/f$  नियंत्रित 3-ph SQIM के साथ 5 kHz और 50 kHz स्विचिंग आवृत्तियों पर लोड के साथ सफलता पूर्वक परीक्षण किया गया है और इसके प्रदर्शन का मूल्यांकन किया गया है। TMS320F28335 का उपयोग ओपन-लूप  $v/f$  नियंत्रण के एल्गोरिथ्म

को लागू करने के लिए एक डिजिटल सिग्नल कंट्रोलर के रूप में किया गया है। प्राकृतिक और मजबूर शीतलन के साथ वीएसआई के गर्मी-सिंक का स्थिर-राज्य तापमान एक थर्मोकपल द्वारा मापा गया है, जबकि वीएसआई लगातार एस क्यूआई एम को 90 मिनट तक चलाता है।

अंतरिक्ष-वेक्टर पल्स-चौड़ाई मॉड्यूलेशन तकनीक का उपयोग आमतौर पर दो-स्तरीय वीएसआई फेड एस क्यू आई एम ड्राइव में किया जाता है जो मुख्य रूप से बेहतर डीसी-बस अनुकूलन के लिए होता है। हालांकि, वीएसआई के पीडब्लूएम आउटपुट वोल्टेज में मुख्य रूप से मौलिक आवृत्ति घटक, वाहक के साइड बैंड में उच्च-क्रम के हार्मोनिक्स और स्विचिंग-थ्रू को रोकने के लिए एवीएसआई में उपयोग किए गए मृत-समय के कारण कुछ कम क्रम के हार्मोनिक्स शामिल हैं। ये उच्च-क्रम स्विचिंग हार्मोनिक्स मुख्य रूप से मुख्य नुकसान (हिस्टैरिसिस और एड़ी चालू नुकसान) और मोटर के अंदर तापमान में वृद्धि करते हैं, और इस प्रकार एस क्यूआई एम ड्राइव की समग्र दक्षता को कम करते हैं। SQIM के स्टेटर-वॉल्टेज के उदय ( $DV / dt$ ) की दर डिवाइस की तेजी से स्विचिंग ट्रांजिस्टर और उच्च स्विचिंग आवृत्ति ऑपरेशन के कारण काफी बढ़ जाती है। यह मूल रूप से घुमावदार इन्सुलेशन विफलता की संभावनाओं को बढ़ाता है, वर्तमान, विद्युत चुम्बकीय चुंबकीय हस्तक्षेप मुद्दों आदि को प्रभावित करता है। इसलिए, वीएसआई और एस क्यू आई एम के बीच साइनसाइडल एलसी फिल्टर नेटवर्क का उपयोग मोटर इनपुट वोल्टेज सिटु से लाल को उच्च-क्रम हार्मोनिक्स में उपस्थित होने के लिए किया जाता है। VSI की पल्स-चौड़ाई संशोधित आउटपुट वोल्टेज। यह मोटर इनपुट वोल्टेज के तेजी से स्विचिंग के संक्रमण को कम करके मोटर के जीवन को भी बढ़ाता है। इस शोध कार्य में, पीडब्लूएम वीएसआई फीडेड एस क्यू आई एम ड्राइव के लिए साइनसाइडल एलसी फिल्टर डिजाइन करने की एक नई पद्धति प्रस्तावित की गई है, जहां रेटेड आवृत्ति पर एस क्यू आई एम की प्रतिक्रियाशील बिजली की मांग के आधार पर फिल्टर कैपेसिटेंस चुना जाता है। हालांकि, प्रस्तावित फिल्टर डिजाइन विधि (PFDM) में फिल्टर इंडक्शन की गणना मानक फिल्टर डिजाइन विधि (SFDM) में फिल्टर इंडक्शन की गणना के समान है। प्रस्तावित नियंत्रण रेखा फिल्टर एक sinusoidal फिल्टर के उद्देश्य को पूरा करता है,  $DV / dt$  को कम करता है, और SQIM की प्रतिक्रियाशील बिजली की मांग की आपूर्ति भी करता है और इस प्रकार इन्वर्टर आउटपुट धाराओं को कम करता है। स्विच करंट के परिमाण पर SFDM और PFDM द्वारा डिजाइन किए गए LC फिल्टर के प्रभाव, ड्राइव में नुकसान, डीसी-लिंक कैपेसिटर का तापमान, मोटर टर्मिनल पर  $DV / dt$ , स्टेटर फ्लक्स और SQIM के एयर-गैप टॉर्क का विश्लेषण किया जाता है। Apposite सिमुलेशन और प्रयोगात्मक परिणामों के साथ। प्रयोग एक प्रयोगात्मक सेट-अप में किए गए हैं जहां विकसित VSI 50 kHz पर स्विच कर रहा है और विभिन्न परीक्षण स्थितियों में ओपन लूप  $v / f$  नियंत्रण

में एक SQIM ड्राइविंग कर रहा है। प्रस्तावित कार्यप्रणाली का उपयोग 5 kHz या 50 kHz पर स्विच करने वाले Si IGBTs या SiC MOSFETs से बने किसी भी VSI के लिए एक साइनसोइडल LC फ़िल्टर को डिज़ाइन करने के लिए किया जा सकता है।

रोटर-फ्लक्स ओरिएंटेड डकंट्रोल (RFOC) में LC फिल्टर के बिना SQIM ड्राइव विभिन्न ऑपरेटिंग बिंदुओं पर एक स्थिर बंद लूप सिस्टम है यदि दो इनर-लूप और दो बाहरी-लूप नियंत्रकों को ठीक से डिज़ाइन किया गया है। हालाँकि, VSI और SQIM के बीच LC फ़िल्टर की शुरुआत, बंद लूप सिस्टम को विभिन्न ऑपरेटिंग बिंदुओं पर अस्थिर कर सकती है जब फ़िल्टर के बिना SQIM के RFOC के लिए पहले से डिज़ाइन किए गए नियंत्रकों के पैरामीटर नहीं बदले जाते। इसलिए, विभिन्न ऑपरेटिंग बिंदुओं पर बंद लूप ड्राइव की अस्थिरता का विश्लेषण एक ही नियंत्रक मापदंडों के साथ किया गया है और यह देखा गया है कि उच्च अस्थिरता प्रतिध्वनि आवृत्ति दोलनों के कारण ऐसी अस्थिरता होती है। इसलिए, चार अलग-अलग सक्रिय भिगोना (AD) विधियाँ उन अस्थिर संचालन बिंदुओं को स्थिर करने के लिए प्रस्तावित की गई हैं जो बिना किसी सक्रिय शक्ति हानि के प्रति ध्वनि आवृत्ति दोलनों को बाहर निकालते हैं। हालाँकि, ये सभी AD विधियाँ SQIM के RFOC की मूल नियंत्रण संरचना और फ़िल्टर के बिना SQIM के RFOC के पहले से डिज़ाइन किए गए आनुपातिक-इंटीग्रल (PI) नियंत्रकों के मापदंडों को नहीं बदलते हैं।

LC फिल्टर के साथ SQIM के RFOC में पहले दो AD विधियों का प्रदर्शन AD विधि में इन्वर्टर-करंट्स का उपयोग करने या LQR का उपयोग करके AD मैट्रिक्स में लाभ मैट्रिक्स की सही गणना पर निर्भर है। इन दो AD विधियों में, किसी भी सक्रिय बिजली के नुकसान के बिना अनुनाद आवृत्ति दोलनों को नम करने के लिए आंतरिक-लूप वर्तमान नियंत्रकों के आउटपुट वोल्टेज संदर्भों से क्षतिपूर्ति की शर्तों को घटाया गया है। हालांकि, ड्राइव के संवेदी अवस्था चर से अनुनाद आवृत्ति घटकों को निकालने के लिए कई उच्च-पास फिल्टर का उपयोग किया गया है और क्षतिपूर्ति की शर्तें तैयार की गई हैं। इसके अलावा, इन AD तरीकों में इन्वर्टर-करंट या सेंसिटिव कैपेसिटर के अलावा वोल्टेज के अलावा SQIM के RFOC में इस्तेमाल किए गए सेंसर के अलावा अतिरिक्त सेंसर की आवश्यकता होती है।

हालाँकि, AD Method III और Method IV, अतिरिक्त सेंसरों की आवश्यकता नहीं है, डंपिंग गेन या लाभ मैट्रिक्स की थकाऊ गणना, अनुनाद आवृत्ति निष्कर्षण के लिए उच्च-पास फिल्टर। AD विधि मूल रूप से अस्थिर संचालन बिंदुओं को स्थिर करने के लिए फ़िल्टर के साथ SQIM के RFOC में आंतरिक स्टेटर-करंट लूप के दो वर्तमान संदर्भों से दो फीड-फॉरवर्ड शब्दों को घटाता है। AD विधि IV मूल रूप से समय की देरी का परिचय देता है और अस्थिर संचालन बिंदुओं को स्थिर करने के लिए आंतरिक स्टेटर-

वर्तमान छोरों को संशोधित करता है। इन विधियों के साथ ड्राइव के प्रदर्शन को सिस्टम के पैरामीट्रिक भिन्नता w.r.t भी सत्यापित किया गया है। फिल्टर के साथ SQIM ड्राइव के संतोषजनक स्थिर-राज्य और गतिशील प्रदर्शन की पुष्टि करने वाले चार एडी तरीकों की प्रभावशीलता को मान्य करने के लिए ड्राइव के विभिन्न परीक्षण स्थितियों में सैद्धांतिक विश्लेषण, कई सिमुलेशन परिणाम, और प्रयोगात्मक परिणाम प्रस्तुत किए गए हैं।

# Table of Contents

CERTIFICATE.....	i
ACKNOWLEDGEMENTS.....	ii
ABSTRACT .....	iv
LIST OF FIGURES .....	xv
LIST OF TABLES.....	xxiii
LIST OF ABBREVIATIONS.....	xxiv
NOMENCLATURE .....	xxvi
Chapter 1.....	1
INTRODUCTION .....	1
1.1 Background and Motivation.....	1
1.2 Design of Three-Phase LC Filters for SQIM Drive .....	3
1.3 Control Methods for SQIM Drive without and with LC Filter .....	5
1.3.1 Control Methods for SQIM Drive without LC Filter.....	5
1.3.2 Control Methods for SQIM Drive with LC Filter.....	7
1.4 Objectives of the Thesis .....	10
1.5 Outline of the Thesis .....	11
Chapter 2.....	13
MODELING AND CONTROL OF SQIM DRIVE WITHOUT AND WITH FILTER .....	13
2.1 Introduction .....	13
2.2 Mathematical Model of SQIM in Stationary Reference (SR) Frame .....	13
2.3 FOC of Induction Motor in Rotor-Flux Reference (RFR) Frame .....	15
2.3.1 Estimation of Rotor Electrical Speed ( $\omega_e$ ) in Sensorless RFOC of SQIM .....	17
2.3.2 Design of Controllers in RFOC of SQIM.....	18
2.3.3 Simulation Results .....	23
2.4 Mathematical Model of LC Filter in SR and RFR Frame .....	27

2.5	Small-Signal Model of SQIM Drive with LC Filter in RFOC .....	28
2.6	Conclusions .....	30
Chapter 3.....		31
DESIGN AND DEVELOPMENT OF SiC VSI AND LC FILTER FOR SQIM DRIVE .....		31
3.1	Introduction .....	31
3.2	Design and Development of SiC MOSFETs Based VSI.....	31
3.2.1	Overview of Power and Sensor Circuits (PSC) .....	32
3.2.2	Considerations in PCB Design of Power and Sensor Circuits (PSC) .....	34
3.2.3	Overview of Gate Driver and Protection Circuits (GDPC) .....	35
3.2.4	Considerations in PCB Design of Gate Driver and Protection Circuits (GDPC) .....	37
3.2.5	Overview of Control Interface and Signal Conditioning Circuits (CISCC) .....	38
3.2.6	Testing of SiC MOSFETs Based VSI with SQIM and Experimental Results.....	39
3.3	Design of Sinusoidal LC Filter for VSI fed SQIM Drive .....	43
3.3.1	Calculation of Filter Inductance ( $L_f$ ) in SFDM and PFDM .....	44
3.3.2	Calculation of Filter Capacitance ( $C_f$ ) in SFDM.....	44
3.3.3	Calculation of Filter Capacitance in PFDM.....	45
3.4	Impacts of LC filter (Theoretical Analysis) .....	47
3.4.1	Reduction of ac-side Current ( $i_{inv}$ ) of VSI.....	47
3.4.2	Reduction of rms Current Ripple and Temperature Rise of dc-link Capacitor.....	48
3.4.3	Reduction of Distortions in Stator-flux of SQIM .....	50
3.4.4	Reduction of Air-gap Torque Pulsation of SQIM.....	50
3.4.5	Reduction of Common-mode Voltage (Special Case).....	51
3.4.6	Reduction of $dv/dt$ at Motor Terminal .....	52
3.5	Impacts of LC filter (Experimental Results) .....	52
3.5.1	Reduction of ac-side Current ( $i_{inv}$ ) of VSI.....	52
3.5.2	Reduction of Temperature of dc-link Capacitor .....	56
3.5.3	Reduction of Distortion in Stator-flux of SQIM.....	59

3.5.4	Reduction of Air-gap Torque Pulsation of SQIM.....	60
3.5.5	Reduction of Common-mode Voltage (Special Case).....	61
3.5.6	Reduction of $dv/dt$ at Motor Terminal .....	62
3.6	Conclusions .....	63
Chapter 4.....		65
STABILIZATION OF SQIM DRIVE WITH LC FILTER IN RFOC: METHOD I AND II.....		65
4.1	Introduction .....	65
4.2	Stability Analysis of SQIM Drive with Filter in RFOC without AD.....	65
4.3	Proposed Active Damping (AD): Method I.....	69
4.3.1	Stability Analysis of Closed-loop Drive with AD Method I .....	70
4.3.2	Simulation Results .....	74
4.3.3	Experimental Results .....	77
4.4	Proposed Active Damping (AD): Method II.....	84
4.4.1	Stability Analysis of Closed-loop Drive with AD Method II .....	85
4.4.2	Simulation Results .....	88
4.4.3	Experimental Results .....	90
4.5	Conclusions .....	91
Chapter 5.....		93
STABILIZATION OF SQIM DRIVE WITH LC FILTER IN RFOC: METHOD III AND IV .....		93
5.1	Introduction .....	93
5.2	Proposed Active Damping (AD): Method III.....	93
5.2.1	Stability Analysis of Closed-loop Drive with FF .....	95
5.2.2	Simulation Results .....	98
5.2.3	Influence of Filter Capacitance Fluctuation.....	101
5.2.4	Experimental Results .....	104
5.3	Proposed Active Damping (AD): Method IV .....	113
5.3.1	Stability Analysis of Closed-loop Drive .....	114

5.3.2	Simulation Results .....	118
5.3.3	Experimental Results .....	122
5.4	Comparison of Four Proposed AD Methods .....	126
5.5	Conclusions .....	128
Chapter 6	.....	130
MAIN CONCLUSIONS AND SCOPE OF FUTURE WORK .....		130
6.1	Main Conclusions.....	130
6.2	Scope of Future Work .....	133
REFERENCES .....		135
LIST OF PUBLICATIONS .....		141

## LIST OF FIGURES

- Fig. 1.1. Block diagram of PWM VSI fed SQIM drive with LC filter.
- Fig. 2.1. Angular orientation of stator-flux and rotor-flux w.r.t the axis of stator and rotor.
- Fig. 2.2. Control block diagram of RFOC of SQIM drive without LC filter.
- Fig. 2.3. Control loop of stator-current of SQIM (a)  $d$ -axis, (b)  $q$ -axis.
- Fig. 2.4. Control loop of magnetizing current of SQIM.
- Fig. 2.5. Control loop of rotor electrical speed of SQIM.
- Fig. 2.6. Speed, stator-current, and magnetizing current of SQIM at its rated speed without and with load torque.
- Fig. 2.7.  $d$ - and  $q$ -axis stator-current, and stator-current of SQIM at its rated speed without and with load torque.
- Fig. 2.8. Speed, stator-current, and magnetizing current of SQIM at low speed without and with load torque.
- Fig. 2.9.  $d$ - and  $q$ -axis stator-current, and stator-current of SQIM at low speed without and with load torque.
- Fig. 2.10. Speed, stator-current, and magnetizing current of SQIM without and with load torque during speed reversal.
- Fig. 2.11.  $d$ - and  $q$ -axis stator-current, and stator-current of SQIM without and with load torque during speed reversal.
- Fig. 2.12. Control loop of stator-current of SQIM with LC filter (a)  $d$ -axis, (b)  $q$ -axis.
- Fig. 3.1. In-house designed and developed 3-ph two-level SiC MOSFETs based VSI.
- Fig. 3.2. Part of Power and Sensor Circuits (PSC).
- Fig. 3.3. Realization of sandwich dc-bus in the PCB of PSC
- Fig. 3.4. Gate driving circuit for switching single SiC MOSFET
- Fig. 3.5. Mechanical cut-out and isolation in GDPC
- Fig. 3.6. Fiber optics transmitters and receivers.
- Fig. 3.7. Line to line voltage waveforms (500 V/div, 10 ms/div) of the VSI feeding the 3-ph SQIM with load at fundamental and switching frequency of 50 Hz and 5 kHz, respectively.

- Fig. 3.8. Line currents (10 A/div, 10 ms/div) of VSI feeding the 3-phase SQIM with load at fundamental and switching frequency of 50 Hz and 5 kHz, respectively.
- Fig. 3.9. Drain to source and gate to source voltages of SiC MOSFET (200 V/div, 10 V/div, 40  $\mu$ s/div) at 5 kHz and dc-link voltage of 600 V.
- Fig. 3.10. Line to line voltages (500 V/div, 10 ms/div) of VSI feeding the 3-phase SQIM with load at fundamental and switching frequency of 50 Hz and 5 kHz, respectively.
- Fig. 3.11. Line currents (10 A/div, 10 ms/div) of VSI feeding 3-phase SQIM with load at fundamental and switching frequency of 50 Hz and 5 kHz, respectively.
- Fig. 3.12. Drain to source and gate to source voltages of SiC MOSFET (200 V/div, 10 V/div, 4  $\mu$ s/div) at 50 kHz and dc-link voltage of 600 V.
- Fig. 3.13. VSI fed three-phase SQIM with sinusoidal LC filter.
- Fig. 3.14. Power circuit considered in SFDM to calculate filter parameters.
- Fig. 3.15. Power circuit considered in PFDM to calculate filter parameters.
- Fig. 3.16. Magnitude of  $i_{inv}$  at variable  $m_l$  and  $f_s$  in (a) SFDM, (b) PFDM.
- Fig. 3.17.  $i_{c,rms}$  at variable  $m_l$  and  $f_s$  in (a) SFDM, (b) PFDM.
- Fig. 3.18. Series-parallel combination of dc-link film capacitor.
- Fig. 3.19. VSI fed 3-ph SQIM with sinusoidal LC filter.
- Fig. 3.20. Sinusoidal LC filters designed by SFDM and PFDM.
- Fig. 3.21.  $i_s$  (2A/div) and  $i_{inv}$  (2A/div) at 50 Hz without filter and light load (a) without filter (b) in SFDM, and (c) in PFDM.
- Fig. 3.22.  $v_{inv(L)}$  (500V/div) and  $v_{s(L)}$  (500V/div) at 50 Hz without filter and light load (a) without filter (b) in SFDM, and (c) in PFDM.
- Fig. 3.23.  $i_s$  (5A/div) and  $i_{inv}$  (5A/div) at 50 Hz without filter and full load (a) without filter (b) in SFDM, and (c) in PFDM.
- Fig. 3.24.  $v_{inv(L)}$  (500V/div) and  $v_{s(L)}$  (500V/div) at 50 Hz without filter and full load (a) without filter (b) in SFDM, and (c) in PFDM.
- Fig. 3.25.  $i_c$  and it's FFT at 50 Hz without filter and light load.
- Fig. 3.26.  $i_c$  and it's FFT at 50 Hz with filter and light load in SFDM.
- Fig. 3.27.  $i_c$  and it's FFT at 50 Hz with filter and light load in PFDM.
- Fig. 3.28.  $i_c$  and it's FFT at 50 Hz without filter and full load.

- Fig. 3.29.  $i_c$  and it's FFT at 50 Hz with filter and full load in SFDM.
- Fig. 3.30.  $i_c$  and it's FFT at 50 Hz with filter and full load in PFDM.
- Fig. 3.31. Stator-flux trajectory of SQIM with light load in (a) SFDM, (b) PFDM.
- Fig. 3.32. Stator-flux trajectory of SQIM with full load in (a) SFDM, (b) PFDM.
- Fig. 3.33. Air-gap torque and its FFT with light load in (a) SFDM, (b) PFDM.
- Fig. 3.34. Air-gap torque and its FFT with full load in (a) SFDM, (b) PFDM.
- Fig. 3.35. Common-mode voltage ( $v_{cm}$ ) w.r.t ground in (a) SFDM, (b) PFDM.
- Fig. 3.36.  $i_{inv}$  and  $i_s$  of VSI and SQIM with the filter at 50 Hz in (a) PFDM, (b) SFDM when “n” is connected with “o”.
- Fig. 3.37. Line to line voltage of VSI and SQIM with the filter in (a) SFDM and (b) PFDM, (c) Line to line voltage of SQIM without and with the filter designed by PFDM.
- Fig. 4.1. Control loop of stator-current of SQIM with filter without AD,  $x = \{d, q\}$ .
- Fig. 4.2. Poles and zeros of  $P_{1d}(s)$  at  $\omega_e = 200$  rad/s without AD.
- Fig. 4.3. Poles and zeros of  $P_{1q}(s)$  at  $\omega_e = 200$  rad/s without AD.
- Fig. 4.4. Waveforms of  $i_{sa}$  and  $v_{sa}$  at  $\omega_e = 200$  rad/s without AD.
- Fig. 4.5. FFT plot of  $v_{sa}$  at  $\omega_e = 200$  rad/s without AD.
- Fig. 4.6. FFT plot of  $i_{sa}$  at  $\omega_e = 200$  rad/s without AD.
- Fig. 4.7. Control block diagram of RFOC of SQIM with LC filter with AD Method I.
- Fig. 4.8. Control loop of stator-current of SQIM with filter with AD,  $x = \{d, q\}$ .
- Fig. 4.9. Waveforms of  $i_{sa}$  and  $v_{sa}$  at  $\omega_e = 200$  rad/s with  $K_{crit}$ .
- Fig. 4.10. Poles and zeros of  $P_{1dm}(s)$  at  $\omega_e = 200$  rad/s with AD.
- Fig. 4.11. Poles and zeros of  $P_{1qm}(s)$  at  $\omega_e = 200$  rad/s with AD.
- Fig. 4.12. Waveforms of  $i_{sa}$  and  $v_{sa}$  at  $\omega_e = 200$  rad/s with AD.
- Fig. 4.13. FFT plot of  $v_{sa}$  at  $\omega_e = 200$  rad/s with AD.
- Fig. 4.14. FFT plot of  $i_{sa}$  at  $\omega_e = 200$  rad/s with AD.
- Fig. 4.15.  $i_{sabc}$ ,  $v_{sabc}$  of SQIM at 250 rad/s where AD is kept on from 0 to 2.5 s and then it is kept off from 2.5 s to 4 s.
- Fig. 4.16. Zoomed version of Fig. 4.15 from 2.46 s to 2.6 s.
- Fig. 4.17.  $\omega_e$ ,  $i_{mr}$ ,  $i_{sabc}$ , and  $v_{sabc}$  in RFOC of drive (SQIM with filter) with AD at 300 rad/s when the load is applied at 2.5 s and removed at 3.5 s.

- Fig. 4.18.  $\omega_e$ ,  $i_{mr}$ ,  $i_{sabc}$ , and  $v_{sabc}$  in RFOC of drive (SQIM with filter) with AD at 32 rad/s when the load is applied at 2.5 s and removed at 3.5 s.
- Fig. 4.19.  $\omega_e$ ,  $i_{mr}$ ,  $i_{sabc}$ , and  $v_{sabc}$  in RFOC of drive (SQIM with filter) with AD when the speed reference is changed at 2 s from 300 to  $-300$  rad/s.
- Fig. 4.20.  $i_{sa}$  and  $v_{sa}$  at  $\omega_e = 100$  rad/s (a) without AD, (b) with AD.
- Fig. 4.21.  $i_{sa}$  and  $v_{sa}$  at  $\omega_e = 200$  rad/s (a) without AD, (b) with AD.
- Fig. 4.22.  $i_{sa}$  and  $v_{sa}$  at  $\omega_e = 250$  rad/s (a) without AD, (b) with AD.
- Fig. 4.23. FFT plot of  $v_{sa}$  at  $\omega_e = 200$  rad/s without AD.
- Fig. 4.24. FFT plot of  $v_{sa}$  at  $\omega_e = 200$  rad/s with AD.
- Fig. 4.25. FFT plot of  $i_{sa}$  at  $\omega_e = 200$  rad/s without AD.
- Fig. 4.26. FFT plot of  $i_{sa}$  at  $\omega_e = 200$  rad/s with AD.
- Fig. 4.27. (a)  $i_{sa}$  (10A/div),  $v_{sa}$  (300V/div), and  $\omega_e$  (100 rad/s) with proposed AD when the electrical speed reference is changed from 32 rad/s to 150 rad/s to 300 rad/s without load, zoomed view at (b) 32 rad/s, (c) 150 rad/s, (d) 300 rad/s.
- Fig. 4.28. (a)  $i_{sa}$  (10 A/div),  $v_{sa}$  (300 V/div), and  $\omega_e$  of SQIM (100 rad/s) with proposed AD when full load is suddenly applied and removed at 300 rad/s, zoomed view at (b) 300 rad/s without load, (c) 300 rad/s with load.
- Fig. 4.29. (a)  $i_{sa}$  (5 A/div),  $v_{sa}$  (50 V/div),  $i_{mr}$  (2.10 A/div), and  $\omega_e$  (50 rad/s) with proposed AD when 85 % load is suddenly applied and removed at 32 rad/s, zoomed view at (b) 32 rad/s without load, (c) 32 rad/s with load.
- Fig. 4.30.  $i_{sa}$  (10A/div),  $v_{sa}$  (300V/div),  $v_{sb}$  (300V/div), and  $\omega_e$  (200 rad/s/div) with proposed AD when electrical speed of SQIM is changed from 300 rad/s to  $-300$  rad/s.
- Fig. 4.31. Transient response of  $i_{sq}$  for three different values of  $K_{damp}$ .
- Fig. 4.32. Control loop of stator-current of SQIM with filter (without LQR),  $x = \{d, q\}$ .
- Fig. 4.33. Modified control loop of stator-current of SQIM with filter (with LQR),  $x = \{d, q\}$ .
- Fig. 4.34. Poles and zeros of  $d$ -axis CLTFs at  $\omega_e = 250$  rad/s without and with LQR.
- Fig. 4.35. Poles and zeros of  $q$ -axis CLTFs at  $\omega_e = 250$  rad/s (without and with LQR).
- Fig. 4.36. Poles and zeros of  $d$ -axis CLTFs at  $\omega_e = 150$  rad/s (without and with LQR).
- Fig. 4.37. Poles and zeros of  $q$ -axis CLTFs at  $\omega_e = 150$  rad/s (without and with LQR).
- Fig. 4.38. Control block diagram of RFOC of SQIM with LC filter with LQR.

- Fig. 4.39.  $\omega_e$ ,  $i_{mr}$ ,  $i_{sabc}$ , and  $v_{sabc}$  in RFOC of the drive (SQIM with filter) with LQR at 300 rad/s when the load is applied at 2.5 s and removed at 3.5 s.
- Fig. 4.40.  $\omega_e$ ,  $i_{mr}$ ,  $i_{sabc}$ , and  $v_{sabc}$  in RFOC of the drive (SQIM with filter) with LQR at 150 rad/s when the load is applied at 2.5 s and removed at 3.5 s.
- Fig. 4.41.  $i_{sa}$  (10A/div),  $v_{sa}$  (500V/div),  $i_{mr}$  (5.56 A/div), and  $\omega_e$  (100 rad/s/div) with LQR when the speed reference is changed from 50 rad/s to 250 rad/s with an intermediate reference of 150 rad/s.
- Fig. 4.42.  $i_{sa}$  (10A/div),  $v_{sa}$  (500V/div),  $i_{mr}$  (5.56 A/div), and  $\omega_e$  (100 rad/s/div) with LQR when the speed reference is fixed at 250 rad/s, and the load is applied at 2.40 s and removed at 6.60 s.
- Fig. 5.1. Control loop of stator-current of SQIM with filter without FF,  $x = \{d, q\}$ .
- Fig. 5.2. Control loop of stator-current of SQIM with filter with FF,  $x = \{d, q\}$ .
- Fig. 5.3. Poles and zeros of  $P_{3d}(s)$  and  $P_{3df}(s)$  at  $\omega_e = 200$  rad/s.
- Fig. 5.4. Poles and zeros of  $P_{3q}(s)$  and  $P_{3qf}(s)$  at  $\omega_e = 200$  rad/s.
- Fig. 5.5. Bode plots of  $P_{1d}(s)$  (blue),  $P_{2d}(s)$  (red), and  $P_{3d}(s)$  (yellow).
- Fig. 5.6. Bode plots of  $P_{31q}(s)$  (blue),  $P_{32q}(s)$  (red), and  $P_{33q}(s)$  (yellow).
- Fig. 5.7. Poles and zeros of  $P_{3d}(s)$  and  $P_{3df}(s)$  at  $\omega_e = 100$  and 250 rad/s.
- Fig. 5.8. Poles and zeros of  $P_{3q}(s)$  and  $P_{3qf}(s)$  at  $\omega_e = 100$  and 250 rad/s.
- Fig. 5.9. Control block diagram of RFOC of SQIM with filter with FF.
- Fig. 5.10. Waveforms of  $i_{sabc}$ ,  $v_{sabc}$  with and without FF at 200 rad/s.
- Fig. 5.11. Reference: 300 rad/s and actual  $\omega_e$ , reference and actual  $i_{mr}$ ,  $i_{sabc}$ , and  $v_{sabc}$  with FF without and with load torque.
- Fig. 5.12. Reference: 63 rad/s and actual  $\omega_e$ , reference and actual  $i_{mr}$ ,  $i_{sabc}$ , and  $v_{sabc}$  with FF without and with load torque.
- Fig. 5.13.  $\omega_e$ ,  $i_{mr}$ ,  $i_{sabc}$ , and  $v_{sabc}$  with FF when the speed reference is changed at 2 s from 200 rad/s to  $-200$  rad/s.
- Fig. 5.14. Poles and zeros of  $P_{df}(s)$  with FF for  $C_f$  of 40  $\mu$ F, 34  $\mu$ F, and 46  $\mu$ F at  $\omega_e = 200$  rad/s.
- Fig. 5.15. Poles and zeros of  $P_{qf}(s)$  with FF for  $C_f$  of 40  $\mu$ F, 34  $\mu$ F, and 46  $\mu$ F at  $\omega_e = 200$  rad/s.

- Fig. 5.16. Poles and zeros of  $P_{df}(s)$  with FF for  $C_f$  of 40  $\mu\text{F}$ , 34  $\mu\text{F}$ , and 46  $\mu\text{F}$  at  $\omega_e = 100$  rad/s.
- Fig. 5.17. Poles and zeros of  $P_{qf}(s)$  with FF for  $C_f$  of 40  $\mu\text{F}$ , 34  $\mu\text{F}$ , and 46  $\mu\text{F}$  at  $\omega_e = 100$  rad/s.
- Fig. 5.18. Poles and zeros of  $P_{df}(s)$  with FF for  $C_f$  of 40  $\mu\text{F}$ , 34  $\mu\text{F}$ , and 46  $\mu\text{F}$  at  $\omega_e = 250$  rad/s.
- Fig. 5.19. Poles and zeros of  $P_{qf}(s)$  with FF for  $C_f$  of 40  $\mu\text{F}$ , 34  $\mu\text{F}$ , and 46  $\mu\text{F}$  at  $\omega_e = 250$  rad/s.
- Fig. 5.20.  $v_{invd}^*$ ,  $v_{invd\_ff}^*$ , and  $i_{sd\_ff}$  at 300 rad/s without and with load torque. (*with filter*)
- Fig. 5.21.  $v_{invq}^*$ ,  $v_{invq\_ff}^*$ , and  $i_{sq\_ff}$  at 300 rad/s without and with load torque. (*with filter*)
- Fig. 5.22. Waveforms of  $v_{invd}^*$ ,  $v_{invd\_ff}^*$ , and  $i_{sd\_ff}$  at 300 rad/s. (*without discrete filter*)
- Fig. 5.23. Waveforms of  $v_{invq}^*$ ,  $v_{invq\_ff}^*$ , and  $i_{sq\_ff}$  at 300 rad/s. (*without discrete filter*)
- Fig. 5.24. Zoomed view of  $v_{invd\_ff}^*$ ,  $i_{sd\_ff}$  without and with discrete filter.
- Fig. 5.25. Zoomed view of  $v_{invq\_ff}^*$ ,  $i_{sq\_ff}$  without and with discrete filter.
- Fig. 5.26.  $v_{sa}$ ,  $i_{sa}$ , and FFT of  $v_{sa}$  at  $\omega_e = 200$  rad/s without FF.
- Fig. 5.27.  $v_{sa}$ ,  $i_{sa}$  and FFT of  $i_{sa}$  at  $\omega_e = 200$  rad/s without FF.
- Fig. 5.28.  $v_{sa}$  and  $i_{sa}$  at  $\omega_e = 200$  rad/s with FF.
- Fig. 5.29.  $v_{sa}$ ,  $i_{sa}$  and FFT of  $v_{sa}$  at  $\omega_e = 100$  rad/s (a) without FF and (b) with FF.
- Fig. 5.30.  $v_{sa}$ ,  $i_{sa}$  and FFT of  $v_{sa}$  at  $\omega_e = 250$  rad/s (a) without FF and (b) with FF.
- Fig. 5.31.  $v_{sa}$  and  $i_{sa}$  with FF at  $\omega_e = 100$  rad/s for (a) 30  $\mu\text{F}$  and (b) 50  $\mu\text{F}$  filter capacitors.
- Fig. 5.32.  $v_{sa}$  and  $i_{sa}$  with FF at  $\omega_e = 200$  rad/s for (a) 30  $\mu\text{F}$  and (b) 50  $\mu\text{F}$  filter capacitors.
- Fig. 5.33.  $v_{sa}$  and  $i_{sa}$  with FF at  $\omega_e = 250$  rad/s for (a) 30  $\mu\text{F}$  and (b) 50  $\mu\text{F}$  filter capacitors.
- Fig. 5.34. (a) Waveforms of  $i_{sa}$ ,  $v_{sa}$ ,  $i_{mr}$ , and  $\omega_e$  with FF at a speed reference of 300 rad/s without load and with full load, (b) Zoomed portion of  $i_{sa}$  and  $v_{sa}$  without load, and (c) Zoomed portion of  $i_{sa}$  and  $v_{sa}$  with load.
- Fig. 5.35. Waveforms of  $i_{sa}$ ,  $v_{sa}$ ,  $v_{sb}$ , and  $\omega_e$  with FF when the speed reference is changed from 200 rad/s to  $-200$  rad/s.
- Fig. 5.36. Waveforms of  $i_{sa}$ ,  $v_{sa}$ , and  $\omega_e$  with FF at a speed reference of 63 rad/s without load and with 80% load, (b) Zoomed portion of  $i_{sa}$  and  $v_{sa}$  without load, and (c) Zoomed portion of  $i_{sa}$  and  $v_{sa}$  with load.

- Fig. 5.37. Control loop of stator-current of SQIM with filter (without MC),  $x = \{d, q\}$ .
- Fig. 5.38. Control loop of stator-current of SQIM with filter (with MC),  $x = \{d, q\}$ .
- Fig. 5.39. Poles and zeros of  $d$ -axis CLTFs at  $\omega_e = 250$  rad/s.
- Fig. 5.40. Poles and zeros of  $q$ -axis CLTFs at  $\omega_e = 250$  rad/s.
- Fig. 5.41. Bode plots of  $P_{41d}(s)$  (blue),  $P_{42d}(s)$  (red), and  $P_{43d}(s)$  (yellow).
- Fig. 5.42. Bode plots of  $P_{41q}(s)$  (blue),  $P_{42q}(s)$  (red), and  $P_{43q}(s)$  (yellow).
- Fig. 5.43. Poles and zeros of  $d$ -axis CLTFs for different  $f_{res}$  at  $\omega_e = 250$  rad/s with MC.
- Fig. 5.44. Poles and zeros of  $q$ -axis CLTFs for different  $f_{res}$  at  $\omega_e = 250$  rad/s with MC.
- Fig. 5.45. Control block diagram of RFOC of SQIM with filter with MC.
- Fig. 5.46.  $i_{sabc}$ ,  $v_{sabc}$  of SQIM at 250 rad/s where MC is kept on from 0 to 2.5 s and then it is kept off from 2.5 s to 4 s.
- Fig. 5.47.  $i_{sd}$  and  $i_{sq}$  of SQIM at 250 rad/s where MC is kept on from 0 to 2.5 s and then it is kept off from 2.5 s to 4 s.
- Fig. 5.48. Zoomed portion of Fig. 5.29 from 2.46 s to 2.6 s.
- Fig. 5.49.  $\omega_e$ ,  $i_{mr}$ ,  $i_{sabc}$ , and  $v_{sabc}$  in RFOC of the drive (SQIM with filter) with MC at 300 rad/s when the load is applied at 2.5 s and removed at 3.5 s.
- Fig. 5.50.  $\omega_e$ ,  $i_{mr}$ ,  $i_{sabc}$ , and  $v_{sabc}$  in RFOC of the drive (SQIM with filter) with MC at 100 rad/s when the load is applied at 2.5 s and removed at 3.5 s.
- Fig. 5.51.  $\omega_e$ ,  $i_{mr}$ ,  $i_{sabc}$ , and  $v_{sabc}$  in RFOC of drive (SQIM with filter) with MC when the speed is reversed at 2.5 s from 300 to  $-300$  rad/s.
- Fig. 5.52.  $v_{sa}$  (200V/div),  $i_{sa}$  (10A/div), and frequency spectrum of  $v_{sa}$  at  $\omega_e = 250$  rad/s without MC.
- Fig. 5.53.  $v_{sa}$  (200V/div),  $i_{sa}$  (10A/div), and frequency spectrum of  $i_{sa}$  at  $\omega_e = 250$  rad/s without MC.
- Fig. 5.54.  $v_{sa}$  (200V/div),  $i_{sa}$  (5A/div) at  $\omega_e = 250$  rad/s with MC.
- Fig. 5.55.  $i_{sa}$  (10A/div),  $v_{sa}$  (500V/div),  $i_{mr}$  (5.56 A/div), and  $\omega_e$  (100 rad/s/div) with LQR when the speed reference is changed from 100 rad/s to 300 rad/s with an intermediate reference of 200 rad/s.
- Fig. 5.56.  $i_{sa}$  (10A/div),  $v_{sa}$  (500V/div),  $i_{mr}$  (5.56 A/div), and  $\omega_e$  (100 rad/s/div) with MC when the speed reference is fixed at 200 rad/s, and the load is applied at 2.70 s and removed at 6.70 s.

Fig. 5.57.  $i_{sa}$  (10A/div),  $v_{sa}$  (200V/div),  $i_{mr}$  (5.56 A/div), and  $\omega_e$  (100 rad/s/div) with MC when the speed reference is fixed at 100 rad/s, and the load is applied at 2.50 s and removed at 6.30 s.

## LIST OF TABLES

Table 1.1	Properties of Si and SiC
Table 2.1	Parameters of 2.2 kW, 415V, 50 Hz, and Four pole SQIM
Table 2.2	Parameters of Four PI Controllers for 5 kHz Switching Frequency
Table 3.1	Parameters of Used SiC MOSFET
Table 3.2	WTHD (%) of Line to Line Voltages of SQIM
Table 3.3	Temperature of Heat Sink in Continuous Run Test of VSI with SQIM
Table 3.4	Parameters of Filter Obtained by SFDM and PFDM
Table 3.5	Comparison with Light Load Torque at 50 Hz
Table 3.6	Comparison with Full Load Torque at 50 Hz
Table 3.7	Loss in VSI and Filter at 50 Hz, Light and Full Load
Table 3.8	Calculated $\Delta T$ in individual Capacitor ( $C_d$ )
Table 3.9	Comparison of Different Components in Torque
Table 3.10	Comparison of Average Torque and Torque Ripple
Table 4.1	Values of $K_{crit}$ at Different Speeds
Table 4.2	Factors Considered in Transient Response of $i_{sq}$
Table 5.1	Phase Margin and Gain margin at Different Cases in Method III
Table 5.2	Phase Margin and Gain Margin at Different Cases in Method IV
Table 5.3	Comparison of Four AD Methods
Table 5.4	Calculation of ITAE, IAE, and ISE for Four AD Methods

## LIST OF ABBREVIATIONS

ASD	Adjustable Speed Drives
AD	Active Damping
BNC	Bayonet Neill-Concelman
CSD	Constant Speed Drives
CMR	Common-Mode Rejection
CCS	Code Composer Studio
CISCC	Control Interface and Signal Conditioning Circuits
CLTF	Closed-Loop Transfer Functions
DTC	Direct Torque control
DSC	Digital Signal Controller
DESAT	Desaturation
DFT	Discrete Fourier Transform
EMI	Electromagnetic Interference
EMC	Electromagnetic Compatibility
ESR	Equivalent Series Resistance
FOC	Field-Oriented Control
FRC	Flat Ribbon Cable
FFT	Fast Fourier Transform
FF	Feed-Forward
GDPC	Gate Driver & Protection Circuits
GM	Gain Margin
IDE	Integrated Development Environment
LQR	Linear Quadratic Regulator
MC	Modified Controllers
PWM	Pulse-Width Modulated
PI	Proportional-Integral
PSC	Power and Sensor Circuits
PFDM	Proposed Filter Design Method
PM	Phase Margin
RMS	Root Mean Square
RFOC	Rotor-Flux Oriented Control
RFR	Rotor-Flux Reference
SQIM	Squirrel Cage Induction Motor
SFDM	Standard Filter Design Method
SiC	Silicon Carbide
Si	Silicon
SPWM	Sinusoidal Pulse Width Modulation

SVPWM	Space Vector Pulse Width Modulation
SFOC	Stator-Flux Oriented Control
SR	Stationary Reference
TFs	Transfer Functions
THD	Total Harmonic Distortion
THB	Temperature Humidity Bias
ULVO	Under-Voltage Lockout
VSI	Voltage Source Inverter
WTHD	Weighted Total Harmonic Distortion

## NOMENCLATURE

$V_{dc}$	dc-link voltage
$f_s$	Fundamental frequency of SQIM
$f_{sw}$	Switching frequency of VSI
$L_f$	Per-phase inductance of filter inductor
$C_f$	Per-phase capacitance of filter capacitor
$R_f$	Per-phase series resistance of filter inductor
$f_{res}$	Effective resonance frequency
$R_s, R_r$	Per-phase stator and rotor resistance of SQIM
$L_{ls}, L_{lr}$	Per-phase stator and rotor leakage inductance of SQIM
$L_s, L_r$	Per-phase stator and rotor self-inductance of SQIM
$L_0$	Per-phase magnetizing inductance of SQIM
$\sigma$	Total leakage factor of SQIM
$\sigma_r$	Rotor leakage factor of SQIM
$\omega_{mr}$	Speed of rotor-flux in synchronously rotating rotor-flux reference frame
$\omega_e$	Electrical speed of the rotor of SQIM
$\omega_r$	Slip speed of SQIM
$J$	Moment of inertia of SQIM
$B$	Friction coefficient of SQIM
$m_d$	Developed electromagnetic torque of SQIM
$m_l$	Externally applied load torque
$P$	Number of poles of SQIM
$\rho_{mr}$	Angle between rotor-flux vector and stator-axis
$\varepsilon$	Angle between stator-axis and rotor-axis
$i_{sa}, i_{s\beta}$	$\alpha$ and $\beta$ components of stator-current in SR frame
$v_{sa}, v_{s\beta}$	$\alpha$ and $\beta$ components of stator-current in SR frame
$\psi_{ra}, \psi_{r\beta}$	$\alpha$ and $\beta$ components of rotor-flux in SR frame
$i_{sd}, i_{sq}$	$d$ - and $q$ -axis components of stator-current
$v_{sd}, v_{sq}$	$d$ - and $q$ -axis components of stator-voltage
$i_{mr}$	Rotor magnetizing current
$v_{ffd}, v_{ffq}$	$d$ - and $q$ -axis feed-forward terms in RFOC
$i_{sa}, i_{sb}, i_{sc}$	$a, b,$ and $c$ phase stator-currents
$v_{sa}, v_{sb}, v_{sc}$	$a, b,$ and $c$ phase stator-voltages
$T_d$	Sampling and transport delay in VSI and DSC
$T_{isd}, T_{isq}$	Time constant of the $d$ - and $q$ -axis stator-current controller
$K_{isd}, K_{isq}$	Gain of the $d$ - and $q$ -axis stator-current PI controller
$K_{imr}$	Gain of the magnetizing current PI controller
$T_{imr}$	Time constant of the magnetizing current PI controller

$K_{\omega}$	Gain of the speed PI controller
$T_{\omega}$	Time constant of the speed PI controller
$i_{in\alpha}, i_{in\beta}$	$\alpha$ and $\beta$ components of inverter-current in SR frame
$v_{in\alpha}, v_{in\beta}$	$\alpha$ and $\beta$ components of inverter-voltage in SR frame
$i_{invd}, i_{invq}$	$d$ - and $q$ -axis components of inverter-current
$v_{invd}, v_{invq}$	$d$ - and $q$ -axis components of inverter-voltage
$i_{inva}, i_{invb}, i_{invc}$	$a$ , $b$ , and $c$ phase inverter-currents
$v_{inva}, v_{invb}, v_{invc}$	$a$ , $b$ , and $c$ phase inverter-voltages
$K_{damp}$	Value of damping gain
$K_{critical}$	Critical value of damping gain
$\zeta$	Damping factor of LC filter